



# Scale Sensitivity of the Gill Circulation. Part I: Equatorial Case

Beatriz Reboredo, Gilles Bellon

## ► To cite this version:

Beatriz Reboredo, Gilles Bellon. Scale Sensitivity of the Gill Circulation. Part I: Equatorial Case. Journal of the Atmospheric Sciences, 2022, 79 (1), pp.3-17. <10.1175/JAS-D-21-0067.1>. <hal-03761067>

**HAL Id: hal-03761067**

**<https://hal.science/hal-03761067v1>**

Submitted on 25 Aug 2022

**HAL** is a multi-disciplinary open access archive for the deposit and dissemination of scientific research documents, whether they are published or not. The documents may come from teaching and research institutions in France or abroad, or from public or private research centers.

L'archive ouverte pluridisciplinaire **HAL**, est destinée au dépôt et à la diffusion de documents scientifiques de niveau recherche, publiés ou non, émanant des établissements d'enseignement et de recherche français ou étrangers, des laboratoires publics ou privés.



HAL Authorization

# Scale Sensitivity of the Gill Circulation. Part I: Equatorial Case

BEATRIZ REBOREDO<sup>a</sup> AND GILLES BELLON<sup>a,b</sup>

<sup>a</sup> *Department of Physics, University of Auckland, Auckland, New Zealand*

<sup>b</sup> *Centre National de Recherches Météorologiques, Université de Toulouse, Météo France, CNRS, Toulouse, France*

(Manuscript received 10 March 2021, in final form 25 August 2021)

**ABSTRACT:** We investigate the steady dynamical response of the atmosphere on the equatorial  $\beta$  plane to a steady, localized, midtropospheric heating source at the equator. Expanding Gill's seminal work, we vary the latitudinal and longitudinal scales of the diabatic heating pattern while keeping its total amount fixed. We focus on characteristics of the response that would be particularly important if the circulation interacted with the hydrologic and energy cycles: the overturning circulation and the low-level wind. In the limit of very small scale in either the longitudinal or latitudinal direction, the vertical energy transport balances the diabatic heating and this sets the intensity of the overturning circulation. In this limit, a fast low-level westerly jet is located around the center of diabatic heating. With increasing longitudinal or latitudinal scale of the diabatic heating, the intensity of the overturning circulation decreases and the low-level westerly jet decreases in maximum velocity and spatial extent relative to the spatial extent of this heating. The associated low-level eastward mass transport decreases only with increasing longitudinal scale. These results suggest that moisture-convergence feedbacks will favor small-scale equatorial convective disturbances while surface-heat-flux feedbacks would favor small-scale disturbances in mean westerlies and large-scale disturbances in mean easterlies. Part II investigates the case of off-equatorial heating.

**KEYWORDS:** Tropics; Atmospheric circulation; Large-scale motions; Shallow-water equations; Monsoons; Idealized models

## 1. Introduction


Gill's (1980, hereafter G80) seminal work aimed to provide a very simple model of the Walker circulation that results from the longitudinal distribution of diabatic heating in the tropics, with maxima of convective heating over the three equatorial landmasses or archipelagos—Amazonia, Africa, and the Maritime Continent (Krueger and Winston 1974)—as well as monsoon circulations resulting from off-equatorial regional diabatic heating. G80 showed that the damped, linear, baroclinic dynamical response of the tropical atmosphere to a localized, steady, midtropospheric diabatic heating reproduces the main features of these circulations.

This simple model has become one of the main frameworks to understand tropical circulations and its solutions are now commonly called Gill circulation. A generalization of G80's work attempted to simulate the seasonal mean flow realistically (Zhang and Krishnamurti 1996), with some success. The relevance of G80's work to the atmospheric circulation associated with El Niño–Southern Oscillation was also revealed soon after the publication of the original article (Pazan and Meyers 1982; Philander 1983). Later studies of the dynamical pattern associated with the Madden–Julian oscillation (MJO) (Madden and Julian 1971; Zhang 2005) revealed that this pattern is essentially G80's equatorially symmetric solution (Hendon and Salby 1994; Kiladis et al. 2005). Very recently,

this framework has shown promise to understand the observed pattern of tropical precipitation in detail (Adam 2018) and the superrotation on tide-locked exoplanets (Showman and Polvani 2010, 2011; Pierrehumbert and Hammond 2019). Because of this widespread relevance, G80's model has come to be considered foundational, and is used as a test for further theoretical development (e.g., Bretherton and Sobel 2003).

One of the main caveat of G80's original model is that it only considers midtropospheric diabatic heating, typically released by condensation associated with deep convection. An alternative framework considers surface sensible heating that ties surface air temperatures to sea surface temperatures, and the corresponding model has shown a dominant role of the surface in driving the pattern of surface convergence, particularly in the tropical eastern Pacific (Back and Bretherton 2009), hence making G80's model less relevant to the Walker circulation than initially concluded. Nevertheless, as pointed by Neelin (1989), G80's model can be interpreted as a surface-forcing model and the two models differ only by the thermodynamic normalization scales and parameters. The pattern and sensitivities of the Gill circulation are therefore also relevant to the surface-forcing model.

G80 mostly focused on two cases, with latitudinal distributions of diabatic heating for which there are simple analytical solutions: one symmetric about the equator, the other anti-symmetric. G80 and Heckley and Gill (1984) presented a few additional cases with little analysis. But observations document diabatic heating patterns with a wide range of horizontal scales and latitudinal locations and we have yet to understand the sensitivity of the Gill circulation to these parameters. The present work aims to understand how the equatorially symmetric Gill circulation depends on the latitudinal and

 Supplemental information related to this paper is available at the Journals Online website: <https://doi.org/10.1175/JAS-D-21-0067.s1>.

*Corresponding author:* Gilles Bellon, [gilles.bellon@auckland.ac.nz](mailto:gilles.bellon@auckland.ac.nz).

*Publisher's Note:* This article was revised on 24 March 2022 to fix Fig. 3, which was incomplete when originally published.

longitudinal scales of the imposed diabatic heating, with a particular focus on characteristics of the circulation that, in the real world, interact with the energy cycle: the vertical, overturning circulation, which is associated with moisture transport and latent heat release, and the surface wind, which modulates the surface turbulent heat fluxes. [Bellon and Reboredo \(2021, hereafter Part II\)](#) investigates the off-equatorial case.

In [section 2](#), we present the solutions to the Matsuno–Gill equations ([Matsuno 1966](#); [G80](#)), as well as the  $f$ -plane case. [Section 3](#) presents some solutions as well as the scale sensitivity of the overturning circulation and low-level wind. [Section 4](#) summarizes our findings and concludes. For brevity, we will refer to “imposed diabatic heating” simply as “heating” in the next sections.

## 2. Method

In this section, we summarize the Matsuno–Gill equations and the method of solution by decomposition in parabolic cylinder functions. We present semianalytical solutions for a more general case than in [G80](#), i.e., applicable to heating of varied horizontal extents and we also derive the asymptotes for small zonal extent of the heating.

### a. The Matsuno–Gill equations

The Matsuno–Gill equations describe the steady first-baroclinic dynamical response of the tropical atmosphere to prescribed midtropospheric heating. They are equivalent to the steady-state, linear, shallow-water equations with damping terms in the zonal-momentum and continuity equations. The linear approximation and the neglect of the momentum damping in the meridional direction (the so-called longwave approximation) are evaluated in the online supplementary material using simplified versions of the quasi-equilibrium tropical circulation models (QTCM) ([Neelin and Zeng 2000](#); [Zeng et al. 2000](#); [Lintner et al. 2012](#)) and they are deemed acceptable for large-scale circulations and realistic amplitudes of heating. Using midtropospheric temperature in the continuity equation instead of pressure (as in [G80](#)) or depth of the layer (as in the shallow-water equations), the Matsuno–Gill equations write

$$\varepsilon u - \frac{1}{2} y v = -\partial_x T, \quad (1)$$

$$\frac{1}{2} y u = -\partial_y T, \quad (2)$$

$$\varepsilon T + \partial_x u + \partial_y v = Q, \quad (3)$$

with  $(u, v)$  the horizontal baroclinic velocity (i.e., the difference between upper-tropospheric and lower-tropospheric velocity),  $T$  the midtropospheric temperature, and  $Q$  the heating. All variables are nondimensional; in particular, distances are normalized by the equatorial radius of deformation, which is about 1000 km. These equations are equivalent to Eqs.

(2.6), (2.8), and (2.12) in [G80](#). The Matsuno–Gill equations have proven successful in explaining observed tropical variability in large part because the gravity wave phase speed, which is the normalizing scale for velocity, is fairly uniform in the tropics as a result of the fairly uniform gross moist stability ([Yu et al. 1998](#)). We take the value of the damping rate  $\varepsilon$  from [G80](#):  $\varepsilon = 0.1$ , which corresponds to a damping time scale of 2.5 days. This damping rate was at times assessed to be too large (e.g., [Battisti et al. 1999](#)) and [Stechmann and Ogrosky \(2014\)](#) suggest that the Walker circulation can be modeled with no damping at all, if only the longitudinal anomaly of heating is imposed and the meridional wind is known. However, other studies suggest that such a large value is justified, in particular because of convective momentum transport ([Lin et al. 2005, 2008](#); [Iipponen and Donner 2021](#)). The sensitivity of the Gill circulation to  $\varepsilon$  is related to that of the zonal scale  $L_x$ , as we show in [section 2d](#).

The nondimensional upward midtropospheric vertical velocity is equal to the nondimensional baroclinic divergence and can be written:

$$w = \partial_x u + \partial_y v = Q - \varepsilon T. \quad (4)$$

If the damping term  $-\varepsilon T$  is interpreted as a local, diabatic, thermodynamic response to the imposed heating  $Q$ , this equation expresses a balance between vertical advection and diabatic heating known as weak-temperature-gradient approximation ([Sobel and Bretherton 2000](#)), although [Bretherton and Sobel \(2003\)](#) interpreted the damping term differently.

[G80's](#) framework assumes that the atmospheric response to the heating has a smaller scale than the planetary scale so that longitudinal and latitudinal boundaries can be considered infinite. The QTCM experiments in the supplementary material, which use realistic boundary conditions, show that this assumption is suitable for realistic horizontal extents of the heating on Earth. This might not hold for larger extents or on exoplanets.

### b. Solutions to cylinder-mode forcing

[G80](#) presented some analytical solutions to Eqs. (1)–(3) for heating patterns that follow:

$$Q^{(n)} = F(x) D_n(y) \text{ with } n \in \mathbb{N}, \quad (5)$$

and  $F$  a half period of cosine function in a limited range of longitude:

$$F(x) = \begin{cases} k \cos(kx) & \text{for } |x| < L_x, \\ 0 & \text{for } |x| > L_x, \end{cases} \quad \text{with } k = \frac{\pi}{2L_x}, \quad (6)$$

and  $D_n$  a parabolic cylinder function of degree  $n$ , i.e., the product of a polynomial of degree  $n$  and an exponential that limits the latitudinal extent of significant heating:

$$\begin{aligned} D_0 &= \exp\left(-\frac{y^2}{4}\right), \\ D_1 &= y \exp\left(-\frac{y^2}{4}\right), \\ D_{n+1} &= y D_n - n D_{n-1}, \quad \forall n > 0. \end{aligned} \quad (7)$$

We will also use  $D_{-1} = D_{-2} = 0$  to write generalized equations. [Appendix A](#) documents some of the properties of these parabolic cylinder functions that we will also call latitudinal modes. Note that our function  $F$  differs from the function  $F$  in [G80](#) by a factor  $k$ , which we introduced to make the integral of  $F$  over the longitude independent of  $L_x$ .

The method of solution as described in [G80](#) introduces two new variables  $q$  and  $r$  that combine  $T$  and  $u$  in Eqs. (1)–(3) as

$$q = T + u, \quad (8)$$

$$r = T - u. \quad (9)$$

For each forcing  $Q^{(n)} = F(x)D_n(y)$  following a latitudinal mode, the solutions  $[q^{(n)}, v^{(n)}, r^{(n)}]$  can be written as the sum of two additive components ([G80](#); [Heckley and Gill 1984](#); [Abramowitz and Stegun 1964](#)),  $[q^{(n,1)}, v^{(n,1)}, r^{(n,1)}]$  and  $[q^{(n,2)}, v^{(n,2)}, r^{(n,2)}]$ , in which  $q^{(n,1)}$  is proportional to  $D_n(y)$  and  $q^{(n,2)} \propto D_{n+2}(y)$ ,  $v^{(n,1)} \propto D_{n-1}(y)$  and  $v^{(n,2)} \propto D_{n+1}(y)$ ,  $r^{(n,1)} \propto D_{n-2}(y)$  and  $r^{(n,2)} \propto D_n(y)$ :

$$\begin{aligned} q^{(n)} &= q^{(n,1)} + q^{(n,2)} = q_n^{(n)}(x)D_n(y) + q_{n+2}^{(n)}(x)D_{n+2}(y), \\ v^{(n)} &= v^{(n,1)} + v^{(n,2)} = v_{n-1}^{(n)}(x)D_{n-1}(y) + v_{n+1}^{(n)}(x)D_{n+1}(y), \\ r^{(n)} &= r^{(n,1)} + r^{(n,2)} = r_{n-2}^{(n)}(x)D_{n-2}(y) + r_n^{(n)}(x)D_n(y). \end{aligned} \quad (10)$$

The functions of longitude  $x$  in the first component are solutions of

$$\text{for } n = 0, \quad \{\varepsilon^2 + k^2\}q_0^{(0)} = \begin{cases} 0 & \text{if } x < -L_x, \\ \varepsilon k \cos(kx) + k^2 \sin(kx) + k^2 \exp[-\varepsilon(x + L_x)] & \text{if } |x| < L_x, \\ 2k^2 \cosh(\varepsilon L_x) \exp\{-\varepsilon x\} & \text{if } x > L_x; \end{cases} \quad (17)$$

$$\text{for } n = 1, \quad q_1^{(1)} = 0; \quad (18)$$

$$\text{for } n > 1, \quad \frac{(2n-1)^2 \varepsilon^2 + k^2}{n-1} q_n^{(n)} = \begin{cases} 2k^2 \cosh[(2n-1)\varepsilon L_x] \exp[(2n-1)\varepsilon x] & \text{if } x < -L_x, \\ (2n-1)\varepsilon k \cos(kx) - k^2 \sin(kx) + k^2 \exp[(2n-1)\varepsilon(x - L_x)] & \text{if } |x| < L_x, \\ 0 & \text{if } x > L_x. \end{cases} \quad (19)$$

Note that only  $q_0^{(0)}$  is nonzero east of the heating region ( $x > L_x$ ), and zero west of it ( $x < -L_x$ ). All other components extend west of the heating region.

It is clear from the similarity of Eqs. (11) and (14) and from the same boundary and continuity conditions that apply to  $q_n^{(n)}$  and  $q_{n+2}^{(n)}$  that the longitudinal dependence of the second component can be written, for all  $n$ :

$$q_{n+2}^{(n)} = \frac{1}{n+1} q_{n+2}^{(n+2)}. \quad (20)$$

$$\frac{dq_n^{(n)}}{dx} - (2n-1)\varepsilon q_n^{(n)} = -(n-1)F(x), \quad (11)$$

$$v_{n-1}^{(n)} = 2n\varepsilon q_n^{(n)} - nF(x), \quad (12)$$

$$r_{n-2}^{(n)} = nq_n^{(n)}. \quad (13)$$

And in the second component, they are solutions of

$$\frac{dq_{n+2}^{(n)}}{dx} - (2n+3)\varepsilon q_{n+2}^{(n)} = -F(x), \quad (14)$$

$$v_{n+1}^{(n)} = 2(n+2)\varepsilon q_{n+2}^{(n)} - F(x), \quad (15)$$

$$r_n^{(n)} = (n+2)q_{n+2}^{(n)}. \quad (16)$$

Solving Eqs. (11) and (14) for  $q_n^{(n)}$  and  $q_{n+2}^{(n)}$  yields the complete solution  $q^{(n)}$  since Eqs. (12), (13), (15), and (16) give  $v_{n-1}^{(n)}$ ,  $v_{n+1}^{(n)}$ ,  $r_{n-2}^{(n)}$ , and  $r_n^{(n)}$  as functions of  $q_n^{(n)}$  and  $q_{n+2}^{(n)}$ . The solutions detailed in [G80](#) are for  $n = 0$  (symmetric heating) and  $n = 1$  (antisymmetric heating).

The longitudinal dependence of the first component can be written:

To get back to the physical nondimensional variables, we use  $T^{(n)} = [q^{(n)} + r^{(n)}]/2$  and  $u^{(n)} = [q^{(n)} - r^{(n)}]/2$ . The first component of the solution is, for  $n = 0$ ,

$$\left. \begin{aligned} u^{(0,1)} &= T^{(0,1)} = \frac{1}{2} q_0^{(0)}(x) D_0(y), \\ v^{(0,1)} &= 0; \end{aligned} \right\} \quad (21)$$

$$\left. \begin{aligned} \text{for } n = 1, \\ u^{(1,1)} &= T_1^{(1,1)} = 0, \\ \text{for } n > 1, \text{ it is } v^{(1,1)} &= -F(x) D_0(y); \end{aligned} \right\} \quad (22)$$

$$\left. \begin{aligned} T^{(n,1)} &= \frac{1}{2} q_n^{(n)}(x) [D_n(y) + n D_{n-2}(y)], \\ u^{(n,1)} &= \frac{1}{2} q_n^{(n)}(x) [D_n(y) - n D_{n-2}(y)], \\ v^{(n,1)} &= n [2 \varepsilon q_n^{(n)}(x) - F(x)] D_{n-1}(y); \end{aligned} \right\} \quad (23)$$

and the solution for the second component is, for all  $n$ ,

$$\left. \begin{aligned} T^{(n,2)} &= \frac{1}{2} q_{n+2}^{(n)}(x) [D_{n+2}(y) + (n+2) D_n(y)], \\ u^{(n,2)} &= \frac{1}{2} q_{n+2}^{(n)}(x) [D_{n+2}(y) - (n+2) D_n(y)], \\ v^{(n,2)} &= [2(n+2) \varepsilon q_{n+2}^{(n)}(x) - F(x)] D_{n+1}(y). \end{aligned} \right\} \quad (24)$$

Following from Eq. (20), it is straightforward that the second component of the temperature and zonal wind response to heating along  $D_n$  has the same pattern as the first component of the response to heating along  $D_{n+2}$ :  $T^{(n,2)} = T^{(n+2,1)}/(n+1)$  and  $u^{(n,2)} = u^{(n+2,1)}/(n+1)$ .

Both components' contributions to the midtropospheric vertical velocity can be written:

$$w^{(n,m)} = \frac{1}{2} F(x) D_n(y) - \varepsilon T^{(n,m)}, \quad (25)$$

for all  $n$  and for  $m = 1$  or  $2$ .

Note the following:

1) Only the first component of the solution for  $n = 0$  extends beyond  $x = L_x$  in the longitudinal direction. It is associated with no meridional wind and has a Kelvin wave structure as noted in G80.

2) All other components have a Rossby wave structure with gyres meridionally aligned in the region  $x < L_x$ , with a westward extent that decreases with  $n$ . On each side of the equator, cyclonic and anticyclonic gyres alternate in the poleward direction.

### c. More general forcing

Because of the variety of scales of diabatic heating in the tropics, it is of interest to understand the dynamical response to heating with a wide range of horizontal extents from the synoptic to the planetary scale. The present work expands on the results of G80 by studying the response to heating  $Q$  with a similar shape as in G80 (half-period cosine in the longitudinal direction, Gaussian in the meridional direction), but with varying longitudinal and latitudinal extents (this Part I) and latitude (Part II).

Let us start with the same longitudinal distribution as in G80 and a very general latitudinal distribution:

$$Q = F(x) D(y), \quad (26)$$

with  $F(x)$  in the form given by Eq. (6), and  $D(y)$  a bounded function of  $y$ .

With inner product  $\langle f, g \rangle = \int f g dy$ ,  $D_n$  functions form an orthogonal basis  $(D_n)_{n \in \mathbb{N}}$ . The norm of each  $D_n$  is  $\sqrt{n! \sqrt{2\pi}}$ .

Any bounded function  $D$  can be decomposed in a series on the basis  $(D_n)_{n \in \mathbb{N}}$ :

$$D(y) = \sum_{n=0}^{\infty} a_n(L_y) D_n(y). \quad (27)$$

It follows that  $Q$  can also be written as a series of  $Q_{n \in \mathbb{N}}^{(n)}$ :

$$Q = \sum_{n=0}^{\infty} a_n Q^{(n)} F(x). \quad (28)$$

Because the Matsuno–Gill equations are linear, the solution to the steady, linear equation set (1)–(3) forced by  $Q = F(x) D(y)$  can be determined semianalytically as a series of the solutions to heating patterns with latitudinal distributions  $D_n$ :

$$\left. \begin{aligned} T &= \sum_{n=0}^{\infty} a_n T^{(n)}, \\ u &= \sum_{n=0}^{\infty} a_n u^{(n)}, \\ v &= \sum_{n=0}^{\infty} a_n v^{(n)}. \end{aligned} \right\} \quad (29)$$

We will study the cases of a Gaussian latitudinal distribution of  $Q$  of varying latitudinal extent centered on latitude  $y_0$ :

$$D(y) = \frac{1}{L_y} \exp \left\{ -\frac{(y - y_0)^2}{4L_y^2} \right\}. \quad (30)$$

With such a formulation, the heating  $Q$  is a “patch” of heating centered on  $(x, y) = (0, y_0)$ . This patch is close to circular for  $L_x = 3L_y$ . By design, the maximum heating varies with  $L_x$  and  $L_y$  in  $k/L_y$ , so that the total heating provided to the atmosphere is independent of the longitudinal and latitudinal scales:

$$[Q] = \int_{-L_x}^{+L_x} \int_{-\infty}^{+\infty} Q dx dy = 4\sqrt{\pi}, \quad (31)$$

with the square brackets  $[\cdot]$  indicating global integration. This allows us to isolate the sensitivity to the scales independently from that to a change in global energy input.

In this Part I, we focus on heating symmetric with respect to the equator, i.e., with  $y_0 = 0$ . The coefficients  $a_n$  are

$$a_{2n} = \frac{1}{2^n n!} \left( \frac{L_y^2 - 1}{L_y^2 + 1} \right)^n \sqrt{\frac{2}{L_y^2 + 1}}, \quad (32)$$

$$a_{2n+1} = 0. \quad (33)$$

In practice, since the infinite sum in Eq. (27) is convergent, it can be approximated by a finite sum up to a value  $m$  following a convergence criterion (Cauchy 1821). The convergence criterion requires to set a positive error of tolerance  $\eta$  for which any index  $l > m$  satisfies  $\left\| \sum_{n=0}^l a_n(L_y) D_n(y) - \sum_{n=0}^{l-1} a_n(L_y) D_n(y) \right\| \leq \eta$ . This value  $m$  will differ for different values of  $L_y$ . For example, setting  $\eta = 0.001$ , one mode is

enough for the trivial case where  $L_y = 1$ , whereas for  $L_y = 0.5$  we need 10 modes to meet the error criterion, and more modes are needed for smaller  $L_y$ . Heckley and Gill (1984) used the same approach to study the transient response to a very localized heating. The results on the Gill circulation presented in this article are the finite-sum approximations of the semianalytical solutions [Eq. (29)], except in the case of the limit  $L_x \rightarrow 0$  for which we can find analytical expressions.

#### d. Limits for heating with small longitudinal extent

Here, we explore the asymptotic solutions for  $L_x \rightarrow 0$ , but this is also relevant for the limit  $\varepsilon \rightarrow 0$ . Indeed, it is easy to write the solutions in Eqs. (17)–(20) as functions of  $\varepsilon L_x$  and  $x/L_x$  [using  $k = \pi/(2L_x)$ ], with no other dependency on  $\varepsilon$  or  $L_x$ . This means that the sensitivity of the solutions to  $\varepsilon$  is the same as the sensitivity to  $L_x$ , except that the patterns scale zonally with  $L_x$ . All the characteristics of the circulation that we study will actually have identical sensitivities to  $\varepsilon$  and to  $L_x$ .

We focus on the interval  $-L_x \leq x \leq L_x$ . Outside this interval, qualitatively, there is subsidence, but there is no simple expression for the solutions. This limit is identical to the limit  $\varepsilon \rightarrow 0$  if we consider the zonal coordinate  $x/L_x$ .

As pointed in G80, the damping in the meridional-momentum equation is negligible only if  $\varepsilon k \ll 1$ . In the limit  $L_x \rightarrow 0$ , this is not verified, so the limit of the Gill circulation for  $L_x \rightarrow 0$  is not well described by the Matsuno–Gill equations. Nevertheless, the supplementary material shows that meridional-momentum damping has a small impact on the Gill circulation down to  $L_x = 0.075$  (or about 70 km), i.e., down to the smallest synoptic scales. Therefore, for large-scale circulations, the asymptote of the solution to the Matsuno–Gill equations for  $L_x \rightarrow 0$  is still relevant.

In this limit,  $k \rightarrow +\infty$  and we have

$$\begin{aligned} q_0^{(0)} &\sim 1 + \sin kx, \\ q_n^{(n)} &\sim (n-1)(1 - \sin kx) \text{ for } n > 0, \\ q_{n+2}^{(n)} &\sim (1 - \sin kx) \text{ for all } n, \end{aligned} \quad (34)$$

for  $|x| \leq L_x$ . Noting that

$$D_n + nD_{n-2} = -\frac{1}{n-1}(D_n - nyD_{n-1}) \text{ for } n > 1$$

and

$$D_{n+2} + (n+2)D_n = D_n + yD_{n+1},$$

we can write the temperature responses to cylindrical forcing as follows:

$$\begin{aligned} T^{(0,1)} &\sim \frac{1}{2}(1 + \sin kx)D_0(y), \\ T^{(1,1)} &\sim 0, \\ T^{(n,1)} &\sim -\frac{1}{2}(1 - \sin kx)[D_n(y) - nyD_{n-1}(y)] \text{ for } n > 1, \\ T^{(n,2)} &\sim \frac{1}{2}(1 - \sin kx)[D_n(y) + yD_{n+1}(y)]. \end{aligned} \quad (35)$$

By combining the odd- $n$  latitudinal modes using Eq. (7), we can further write

$$T^{(0)} \sim \frac{1}{2}(1 - \sin kx)y^2 D_0(y) + D_0(y), \quad (36)$$

$$T^{(n)} \sim \frac{1}{2}(1 - \sin kx)y^2 D_n(y) \text{ for } n > 0. \quad (37)$$

By multiplying  $T^{(n)}$  by  $a_n$  and summing over  $n$ , we get the asymptote of the solution  $T$  for  $L_x \rightarrow 0$ :

$$T \sim \frac{1}{2}(1 - \sin kx)y^2 D(y) + a_0 D_0(y). \quad (38)$$

This result is valid for any bounded function  $D$ , not only the Gaussian distribution given in Eq. (30). A scale analysis reveals the first order for  $w$ :  $\varepsilon T = \mathcal{O}(D)$ , while  $Q = \mathcal{O}(D/L_x)$  so that  $\varepsilon T \ll Q$  and

$$w \sim k \cos(kx) D(y) = Q, \quad (39)$$

which expresses a balance between heating and transport.

The asymptotes for the zonal and meridional winds can be obtained using Eqs. (1) and (2):

$$u \sim -2(1 - \sin kx) \left[ D(y) + \frac{y}{2} \frac{dD}{dy} \right] + a_0 D_0(y), \quad (40)$$

$$v \sim -k \cos(kx) y D(y), \quad (41)$$

valid for any bounded function  $D$ . For heating following a Gaussian distribution symmetric about the equator [Eq. (30) with  $y_0 = 0$ ], which is the case of interest in this Part I, Eq. (40) further simplifies into

$$u \sim -2(1 - \sin kx) \left( 1 - \frac{y^2}{4L_y^2} \right) D(y) + a_0 D_0(y), \quad (42)$$

which is negative around the heating center, indicating upper-tropospheric easterlies and low-level westerlies in this region. The zonal wind is maximum on the equator at the western boundary of the heating region ( $x = -L_x$ ), and it decreases both eastward and poleward, eventually changing sign.

If  $L_y \rightarrow 0$  as well, all the results above hold, and the last term on the right-hand side of Eq. (42) is negligible: the equatorial zonal wind scales with  $1/L_y$  and the jets extends in longitude all the way to the eastern boundary of the heating region ( $x = L_x$ ) and in latitude to  $y = \pm 2L_y$  on both sides of the heating center. This limit shows that the Gill response is zonally asymmetric even for scales that are much smaller than the equatorial radius of deformation: it is characterized by a westerly low-level jet at the heating center. This suggests significant limitations on the approach considering that small systems in the equatorial regions are well approximated by nonrotating systems.

#### e. A baseline: The $f$ -plane case

The zonal asymmetry that is characteristic of the Gill circulation results from the  $\beta$  effect. This calls for a further evaluation of



this effect. To do so, we also present some elements of the solution on an  $f$  plane. In this case, the solution is a damped inertio-gravity wave. Equations for momentum and continuity reduce to

$$w = -\frac{\varepsilon}{\varepsilon^2 + f^2} \nabla T, \quad (43)$$

$$T = \frac{1}{\varepsilon} Q + \frac{1}{\varepsilon^2 + f^2} \nabla T, \quad (44)$$

in which  $\nabla$  is the Laplacian operator. In the equatorial case,  $f = 0$ , i.e., rotation is neglected, and the solution is a damped gravity wave, in which the horizontal wind is exclusively divergent.

These equations make clear that, in the absence of any circulation, the temperature response is the direct thermodynamic response  $Q/\varepsilon$ . Vertical energy transport appears as a diffusive term  $\Delta T/(\varepsilon^2 + f^2)$  that damps temperature gradients and makes the equilibrium temperature response to heating spatially smoother than the heating itself. Both the ascending motion and diffusive effect are larger in the equatorial case ( $f = 0$ ) than in the off-equatorial case ( $f \neq 0$ ).

Scale analysis allows us to establish the asymptote of this solution for small horizontal extent of the heating, if  $L_x \rightarrow 0$  (or  $L_y \rightarrow 0$ , since this set of equations is isotropic). If the scaling of the temperature is  $\mathcal{T}$ , the scaling of the diffusive term on the right-hand side of Eq. (44) is

$$\frac{1}{\varepsilon^2 + f^2} \nabla T \sim \frac{1}{\varepsilon^2 + f^2} \frac{\mathcal{T}}{L_x^2} \gg \mathcal{T}. \quad (45)$$

Consequently, the term on the left-hand side of Eq. (44) is negligible, and this equation shows a balance between vertical transport and heating  $w \sim Q$  in the limit of very small horizontal extents of the heating, as for the Gill circulation.

### 3. Results

#### a. Temperature and wind response

Here, we present the features of the solutions in terms of temperature, surface winds, and midtropospheric vertical motion for heating distributions  $Q$  with a few different horizontal extents. Figure 1 depicts contours of temperature perturbation and surface velocity field for the Gill circulation forced by heating of different meridional scales, but with the same total, horizontally integrated heating  $[Q]$ :  $L_y = 1$  (equatorial radius of deformation, Fig. 1a),  $L_y = 1/2$  (Fig. 1b), and  $L_y = 1/4$  (Fig. 1c), with a fixed aspect ratio so that  $L_x = 3L_y$  (corresponding to a heating pattern close to circular). Figure 2 shows the corresponding contours of midtropospheric vertical velocity together with contours of heating. Figures 1a and 2a are almost identical to the symmetric forcing presented in G80, the only difference being the longitudinal extent:  $L_x = 3$  here while G80 showed solutions for  $L_x = 2$ .

As expected, the Gill circulation exhibits Kelvin wave easterlies east of the heating region and cyclonic gyres straddling the equator west of it, with maxima of temperature at the center of the gyres (Fig. 1). As the horizontal extent of the heating is decreased, winds get stronger, especially the equatorial

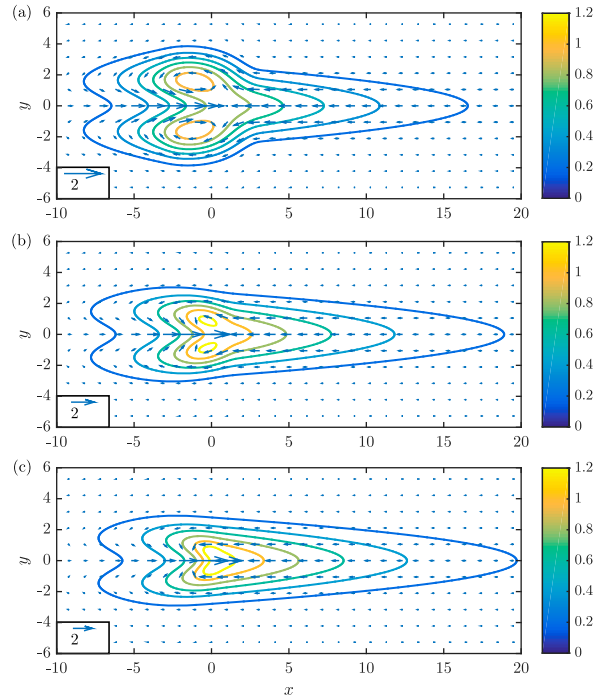


FIG. 1. Solutions for the Gill circulation: temperature response (contours) and low-level velocity (vectors) for (a)  $L_y = 1$  (equatorial radius of deformation), (b)  $L_y = 1/2$ , and (c)  $L_y = 1/4$ . In all cases,  $L_x = 3L_y$ .

westerly jet between the gyres, and the off-equatorial temperature maxima move closer to the equator, they even merge for small  $L_y$  (Fig. 1). As the horizontal extent of the heating is decreased, the maximum vertical speed increases faster than the maximum heating, which scales with  $L_x^{-1} L_y^{-1}$ , and the vertical speed pattern becomes more similar to that of the heating (Fig. 2).

Overall, the meridional extent of the response decreases. The eastward extent of the temperature and horizontal-wind response increases and the westward extent decreases slightly with decreasing horizontal extent of heating (Fig. 1). This reveals a decrease in the Rossby wave response in the west, while the Kelvin wave response expands eastward. The latter corresponds to an increase in the projection of  $D$  on  $D_0$  with decreasing  $L_y$ , which is consistent with the expression of  $a_0$  [see Eq. (27)].

#### b. Overturning circulation

One of the most important characteristics of a tropical circulation is its overturning mass flux, because of its potential interaction with the hydrologic cycle. We define the intensity of the overturning circulation  $\Gamma$  as the upward vertical mass flux integrated over the horizontal domain (which, by mass conservation, is the same as the downward vertical mass flux integrated over the domain):

$$\Gamma = \int \int_{w>0} w \, dx \, dy. \quad (46)$$

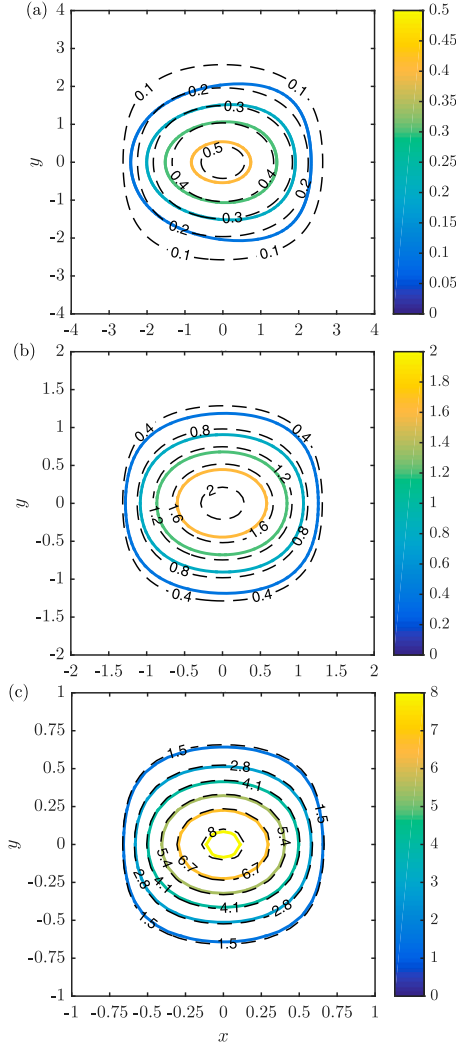


FIG. 2. Forcing and solution for the Gill circulation: heating (dashed lines) and midtropospheric vertical velocity (solid lines) for (a)  $L_y = 1$ , (b)  $L_y = 1/2$ , and (c)  $L_y = 1/4$ . In all cases,  $L_x = 3L_y$ .

The value of  $\Gamma$  can be computed numerically using the expression of  $w$  in Eq. (25).

Figure 3a shows the intensity  $\Gamma$  of the overturning circulation, as a function of the characteristic extents of heating  $L_x$  and  $L_y$ . For  $L_x \rightarrow 0$  or  $L_y \rightarrow 0$ ,  $\Gamma$  has the same limit. As shown in section 2d, in the limit  $L_x \rightarrow 0$ ,  $w \sim Q > 0$  in the heating region and by spatial integration,  $\Gamma \sim [Q]$ . It appears that  $\Gamma$  has the same limit for  $L_y \rightarrow 0$ .

The  $f$ -plane case described in section 2e sheds some light on this: the damped inertio-gravity wave presents the same limit for  $w \sim Q$  for  $L_x$  or  $L_y \rightarrow 0$ , and therefore also  $\Gamma \sim [Q]$ . For small-scale heating, the heating  $Q$  and the local temperature response to this heating  $Q/\varepsilon$  are very peaked at the center of heating, the diffusive transport is therefore very efficient at reducing the temperature response, so efficient that the resulting temperature perturbation is negligible

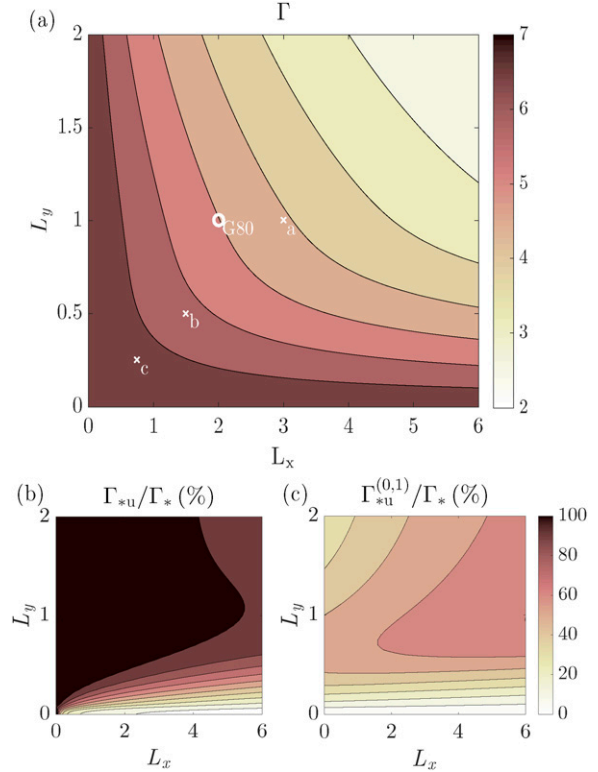


FIG. 3. (a) Intensity  $\Gamma$  of the overturning circulation; the letters “a,” “b,” and “c” indicate the cases shown in Figs. 1 and 2, and “G80” indicates the case discussed in G80 (contours interval 0.5); (b) contribution  $\Gamma_{*u}$  of the zonal flow to the overturning circulation (in % of  $\Gamma_*$ ); and (c) contribution  $\Gamma_{*u}^{(0,1)}$  of the easterly flow to the overturning circulation (in % of  $\Gamma_*$ ).

compared to  $Q$  and the main balance is between vertical energy transport and heating ( $w \sim Q$ ). We hypothesize that the physical mechanism is the same in the Gill circulation for both  $L_x \rightarrow 0$  and  $L_y \rightarrow 0$ .

$\Gamma$  decreases with increasing  $L_x$  and  $L_y$ , in a similar fashion for both scales [for  $L_y = 1$ , the sensitivity to  $L_x$  is also documented in Iipponen and Donner (2021)]. There are two factors contributing to this:

- First, even without rotation (i.e., the  $f$ -plane case detailed in section 2e with  $f = 0$ )  $\Gamma$  decreases with increasing horizontal extent of the heating. Indeed, as the horizontal extent increases,  $Q$  becomes spatially smoother because  $[Q]$  is fixed. As a result, the diffusive effect of large-scale transport becomes less efficient at damping the temperature response.  $W = Q - \varepsilon T$  becomes smaller, and by spatial integration, this decrease is transmitted to  $\Gamma$ . A similar sensitivity to zonal scale and vertical scales was found by Iipponen and Donner (2021) for a nonrotating, meridionally averaged model of the Walker circulation.
- Rotation increases the sensitivity of the overturning circulation to the horizontal extent of the heating pattern. Indeed, Fig. 1 shows that rotation creates gyres straddling the equator, which are mostly rotational, while the damped gravity



wave is exclusively divergent. The poleward flow associated with these gyres compensates most of their equatorward flow and we expect the meridional wind to contribute little to the divergence of the horizontal wind and associated upward motion. We can also propose an energetic interpretation of this sensitivity.<sup>1</sup> The energy source of the system is the heating, and the sinks are the kinetic energy loss through Rayleigh friction and the thermal energy loss through Newtonian cooling, the sum of which is proportional to the total energy (kinetic plus thermal). Assuming the global thermal energy (and thermal energy loss) does not vary significantly with rotation, the global kinetic energy should be similar with and without rotation. Without rotation, all kinetic energy corresponds to divergent motion while in the rotating case part of it is associated with rotational motion and the kinetic energy of divergent motion is smaller than without rotation. We can therefore expect the divergent flow to be weaker with rotation than without.

A more quantitative understanding of  $\Gamma$  can be hindered by the fact that the domain of integration in Eq. (46) is determined by the field  $w$  itself, which we know only as a sum. But Fig. 2 suggests that the upward motion is limited to a region between  $-L_x$  and  $L_x$  in longitude, with a meridional extent that scales with  $L_y$ . We find that  $\Gamma$  can be approximated by the integral  $\Gamma_*$  of  $w$  over the domain  $[-L_x, L_x], [-4L_y, 4L_y]$ , with the latitudinal bounds corresponding to twice the  $e$ -folding distance of  $D$ :

$$\Gamma_* = \int_{-4L_y}^{4L_y} \int_{-L_x}^{L_x} w \, dx \, dy \approx \Gamma. \quad (47)$$

Approximating  $\Gamma$  by  $\Gamma_*$  introduces an error that is small (<5%) for most relevant values of  $L_x$  and  $L_y$ , but becomes

larger if both  $L_x$  and  $L_y$  are large. It is up to 16%, for the maximum values we have considered  $\sim (L_x, L_y) = (6, 2)$ ; nevertheless, combinations of such large values of  $L_x$  and  $L_y$  are outside the observed range ( $L_x = 6$  corresponds to more than a quarter of Earth's circumference and  $L_y = 2$  to heating that extend to the extratropics in both hemispheres), and  $\Gamma_*$  is therefore a reasonable approximation to  $\Gamma$  for realistic extents of  $Q$ . This approximation allows us to decompose the intensity of the overturning circulation into the sum of contributions from the different latitudinal modes:

$$\Gamma_* = \sum_{n=0}^{\infty} \Gamma_*^{(2n)} = \sum_{n=0}^{\infty} \Gamma_*^{(2n,1)} + \Gamma_*^{(2n,2)}, \quad (48)$$

with  $\Gamma_*^{(2n,1)}$  and  $\Gamma_*^{(2n,2)}$  the contributions of the first and second part of the response to the projection of the heating latitudinal distribution  $D$  on the  $n$ th symmetric latitudinal modes  $D_{2n}$ , i.e.,  $a_{2n}$  multiplied by the response to heating in the form  $F(x)D_{2n}(y)$ :

$$\Gamma_*^{(2n,i)} = a_{2n} \int_{-4L_y}^{4L_y} \int_{-L_x}^{L_x} w^{(2n,i)} \, dx \, dy, \quad (49)$$

for  $i = 1, 2$ . Appendix B shows that we can write these contributions as

$$\Gamma_*^{(2n,1)} = \gamma_{2n}(L_x) f_{2n}(L_y) + [1 - \gamma_{2n}(L_x)] g_{2n,1}(L_y), \quad (50)$$

$$\Gamma_*^{(2n,2)} = \gamma_{2n+2}(L_x) f_{2n}(L_y) + [1 - \gamma_{2n+2}(L_x)] g_{2n,2}(L_y), \quad (51)$$

with the variation in  $L_x$  given by the series of functions  $\gamma_{2n}$ :

$$\begin{aligned} \gamma_0 &= \frac{1}{2} q_0^{(0)}(L_x) = \frac{1}{2} \frac{1 + e^{-2\epsilon L_x}}{1 + \epsilon^2 L_x^2}, \\ \gamma_{2n} &= \frac{1}{2} \frac{q_{2n}^{(2n)}(-L_x)}{2n-1} = \frac{1}{2} \frac{q_{2n}^{(2n-2)}(-L_x)}{2n-1} = \frac{1}{2} \frac{1 + e^{-2(4n-1)\epsilon L_x}}{1 + (4n-1)^2 \epsilon^2 L_x^2} \text{ for } n > 0, \end{aligned} \quad (52)$$

with  $l_x = 1/k = 2L_x/\pi$ ; and the variation in  $L_y$  given by

$$f_{2n} = a_{2n}(L_y) I_{2n} \text{ with } I_{2n} = \int_{-4L_y}^{4L_y} D_{2n} \, dy, \quad (53)$$

$$g_{2n,1} = -\frac{8n}{4n-1} a_{2n}(L_y) D_{2n-1}(4L_y), \quad (54)$$

and

$$g_{2n,2} = \frac{4}{4n+3} a_{2n}(L_y) D_{2n+1}(4L_y). \quad (55)$$

Figure 4 shows these functions for  $n \leq 5$ . In terms of amplitude,  $\Gamma_*$  is dominated by the response of mode  $n = 0$ , because the differences  $f_0 - g_{0,1} = f_0$  and  $f_0 - g_{0,2}$  are the largest, and because  $\gamma_0$ 's decrease with increasing  $L_x$  is the slowest of all  $\gamma_{2n}$ . But in terms of sensitivity to  $L_x$  and  $L_y$ , modes with larger  $n$  contribute significantly.

Since  $\gamma_{2n}(0) = 1$ ,  $\Gamma_*^{(2n,i)}(0, L_y) = f_{2n}$  for all  $n$  and  $i = 1, 2$ ; we can establish that

$$\Gamma_*(0, L_y) = 2 \int_{-4L_y}^{4L_y} \sum_{n=0}^{\infty} a_{2n} D_{2n} \, dy = 2 \int_{-4L_y}^{4L_y} D \, dy = \text{erf}(2)[Q], \quad (56)$$

which is a good approximation to  $\Gamma(0, L_y) = [Q] (\text{erf}(2) \approx 0.995)$ . This limit is independent of  $L_y$ , which is consistent with Fig. 3a.  $\Gamma_*$  also appears to tend toward a value close to  $[Q]$  for  $L_y \rightarrow 0$ .

<sup>1</sup> The supplementary material shows that our quasi-analytical solutions to the linear equations with the longwave approximation are very similar to the numerical solutions to the full nonlinear, energy-conserving equations, which shows that our equations approximately satisfy energy conservation and energy-based reasoning is sound.

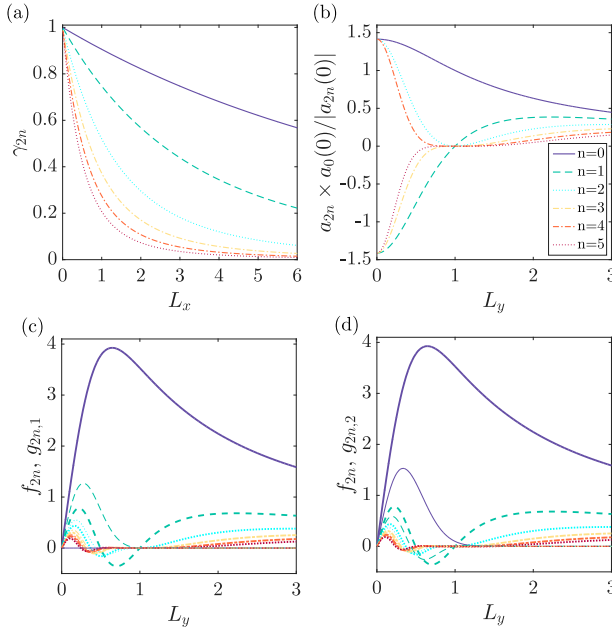


FIG. 4. Functions determining the sensitivity of the contribution  $\Gamma_{*}^{(2n,i)}$  to the longitudinal extent  $L_x$  and  $L_y$  of heating for  $n \leq 5$ : (a)  $\gamma_{2n}(L_x)$  gives the variation of  $\Gamma_{*}^{(2n,1)}$  and  $\Gamma_{*}^{(2n-2,2)}$  from the  $f_{2n}$  for  $L_x = 0$  to, respectively,  $g_{2n,1}$  and  $g_{2n,2}$  for  $L_x \rightarrow \infty$ ; (b)  $a_{2n}$  the projection coefficient of  $D$  on the latitudinal mode  $D_{2n}$ , normalized by  $|a_{2n}(0)/a_0(0)|$ ; (c)  $f_{2n}$  (thick lines) and  $g_{2n,1}$  (thin lines) give the limits of  $\Gamma_{*}^{(2n,1)}$  for, respectively,  $L_x = 0$  and  $L_x \rightarrow \infty$ ; and (d)  $f_{2n}$  (thick lines) and  $g_{2n,2}$  (thin lines) give the limits of  $\Gamma_{*}^{(2n,2)}$  for, respectively,  $L_x = 0$  and  $L_x \rightarrow \infty$ .

With  $\gamma_{2n} \rightarrow 0$  for  $L_x \rightarrow \infty$ , each contribution  $\Gamma_{*}^{(2n,i)}$  tends toward  $g_{2n,i}$  for  $L_x \rightarrow \infty$ . Figure 4a shows the functions  $\gamma_{2n}$  for  $n$  from 0 to 5. The decrease of  $\gamma_0$  with  $L_x$  results from the sensitivity of the diffusive effect of large-scale circulation described above (since the first component of the response to  $D$ 's projection onto  $D_0$  is a damped Kelvin wave,  $\Gamma_{*}^{(0,1)}$  is not affected by rotational effects). The decay of  $\gamma_{2n}$  with  $L_x$  is increasingly fast with increasing  $n$ , which means that the larger  $n$  (and the larger  $i$ ), the faster the convergence of  $\Gamma_{*}^{(2n,i)}$  toward its limit  $g_{2n,i}$  for  $L_x \rightarrow \infty$ . A more intricate latitudinal structure of heating (i.e., a larger  $n$ ) yields a stronger sensitivity of the circulation response to  $L_x$ . We can attribute this change in sensitivity to the effect of rotation: for larger  $n$ , the heating pattern has extrema farther from the equator, where the effect of rotation is larger and temperature anomalies generate circulations that are increasingly rotational and less and less convergent, creating less vertical motion.

From its value for  $L_x = 0$  independent of  $L_y$  [see Eq. (56)], the decrease of  $\Gamma_{*}$  with  $L_x$  is determined by the circulation responses to heating along  $D_{2n}$ ,  $f_{2n}(L_y)$  for  $L_x = 0$ , and  $g_{2n,i}(L_y)$  for  $L_x \rightarrow \infty$ . The sensitivity of these functions  $f_{2n}$  and  $g_{2n,i}$  to  $L_y$  result from (i) the change in projection of  $D$  onto the latitudinal modes  $D_{2n}$ , given by  $a_{2n}$ , and (ii) the extension of the horizontal domain of integration ( $[-L_x, L_x]$ ,  $[-4L_y, 4L_y]$ ) with  $L_y$ . Figures 4b–4d show functions  $f_{2n}(L_y)$  and  $g_{2n,i}(L_y)$ . We can distinguish two domains:

- $L_y \geq 1$ : for  $L_y = 1$ ,  $D = D_0$ —this is the case described in G80. For increasing  $L_y > 1$ ,  $D$  is less and less peaked at the equator; it projects increasingly on higher-and-higher- $n$   $D_n$  while projecting less and less on  $D_0$ , as shown in Fig. 4b. Because of the exponential decay of  $D_n(4L_y)$  with increasing  $L_y$ ,  $g_{2n,1}$  and  $g_{2n,2}$  are negligible in this range of  $L_y$  (see Figs. 4c,d); for the same reason,  $I_{2n}$  is similar to its limit  $I_{2n}^{\infty}$  for  $L_y \rightarrow \infty$ . As a result,  $\Gamma_{*}^{(2n,i)} \approx \gamma_{2(n+i-1)}(L_x)a_{2n}(L_y)I_{2n}^{\infty}$  and its variation with  $L_y$  is mostly determined by the variation of  $a_{2n}$  (see Figs. 4b–d), with a decreasing contribution of mode 0 and an increasing contribution of higher and higher  $n$  modes for increasing  $L_y$ . Considering the sensitivity of the functions  $\gamma_{2n,i}(L_x)$  to  $n$  explained above, the decrease of  $\Gamma_{*}$  with  $L_x$  is therefore larger for larger  $L_y$ . Since  $\Gamma_{*}$  is independent of  $L_y$  for  $L_x = 0$ , this explains the sensitivity of  $\Gamma_{*}$  to both  $L_x$  and  $L_y$ .
- $L_y < 1$ : there is still a strong influence of the response of mode  $n = 0$  and the influence of modes with larger  $n$  is complex. For  $L_y$  close to zero, both  $a_{2n}(0)$  and  $I_{2n} \approx 8L_y D_{2n}(0)$  alternate sign as  $(-1)^n$  [see Eqs. (27) and (5)], so  $f_{2n}$  is positive for all  $n$ . But  $f_{2n} - g_{2n,1}$  is negative for  $n > 0$ , which means that the contributions to the circulation  $\Gamma_{*}^{(2n,1)}$  increases with increasing  $L_x$ .  $f_{2n} - g_{2n,2}$  is positive and  $\Gamma_{*}^{(2n,2)}$  decreases with increasing  $L_x$  and compensates the increase of  $\Gamma_{*}^{(2n,1)}$ . For  $L_y$  closer to 1,  $f_{2n}$ ,  $g_{2n,1}$ ,  $g_{2n,2}$ , and their differences can change sign for  $n > 0$  since  $D_{2n}$  and  $D_{2n+1}$  changes sign at least once over the interval  $[-4L_y, 4L_y]$ , resulting in an increase of the contributions  $\Gamma_{*}^{(2n,i)}$  with increasing  $L_x$  in intervals where  $a_{2n}(f_{2n} - g_{2n,i}) < 0$ . These contributions in these intervals reduce the sensitivity of  $\Gamma_{*}$  to  $L_x$  and, since  $\Gamma_{*}(0, L_y)$  is a constant,  $\Gamma_{*}$  for  $L_x \neq 0$  is larger for reduced sensitivity to  $L_x$ , i.e., for smaller  $L_y$ .

Despite this overall complexity, it appears clearly that the two components of the response to heating along  $D_0$  are the main contributors to  $\Gamma_{*}$  and its sensitivity. This is because in this mode, the Kelvin wave pattern and the Rossby wave pattern both contribute to low-level wind convergence in the region of ascent through the easterlies at the eastern boundary (for the first component) and westerlies at the western boundary (for the second component). By contrast, the two components for modes with  $n > 0$  are opposite close to the equator, with gyres that circulate in opposite directions, and there is a significant amount of compensation between components of the response to heating along  $D_{2n}$  with  $n > 0$ .

Thanks to the continuity equation, we can also decompose  $\Gamma_{*}$  into the sum of a contribution from the meridional wind ( $v$  integrated over the boundary at  $y = \pm 4L_y$ ) and a contribution  $\Gamma_{*u}$  from the zonal wind ( $u$  integrated over the boundaries at  $x = \pm L_x$ ). And each contribution  $\Gamma_{*}^{(2n,i)}$  can also be decomposed in the same way:

$$\Gamma_{*} = \Gamma_{*u} + \Gamma_{*v} \text{ and } \Gamma_{*}^{(2n,i)} = \Gamma_{*u}^{(2n,i)} + \Gamma_{*v}^{(2n,i)}.$$

$$I_{2n}^{\infty} = \sqrt{\pi}(2n)!/2^{n-1}n!.$$

Because  $u^{(0,1)}(-L_x) = 0$  and  $u^{(2n,i)}(L_x) = 0$  for all  $n > 0$  or  $i = 2$ , the contribution from the zonal wind at the eastern border results exclusively from the damped Kelvin wave extending eastward from the heating region, while the contribution from the zonal wind at the western border results from a combination of damped Rossby waves. By integrating  $u$  given in Eqs. (21)–(24), we can write (see last paragraph of [appendix B](#))

$$\Gamma_{*u}^{(2n,1)} = \gamma_{2n}(L_x) \left[ f_{2n}(L_y) - (4n-1)g_{2n,1}(L_y) \right], \quad (57)$$

$$\Gamma_{*u}^{(2n,2)} = \gamma_{2n+2}(L_x) \left[ f_{2n}(L_y) + (4n+3)g_{2n,2}(L_y) \right], \quad (58)$$

and we can compute  $\Gamma_{*u}$  by summing over  $n$ . [Figure 3b](#) shows that except for small  $L_y$ ,  $\Gamma_{*u}$  is the dominant contribution to  $\Gamma_*$ . The smaller contribution of the meridional wind  $\Gamma_{*v}$  results from the partial compensation between the equatorward and poleward branches of the gyres. And the westerly low-level zonal flow into the ascending region through its western boundary, which is also part of these gyres, contributes very significantly to the overturning circulation. In the limit  $L_x \rightarrow 0$ ,  $\Gamma_* \approx \Gamma_{*u}$ . [Section 2d](#) also shows that, in this limit,  $w \sim Q$ ; this means that the region of ascent is the region of heating that extends to infinity in the latitudinal direction, so that there is no flow at the meridional boundaries:

$$\Gamma_u \sim \Gamma \sim [Q] \text{ and } \Gamma_v \sim 0 \quad (59)$$

irrespective of  $L_y$ : this result is valid for both  $\Gamma$  and its approximation  $\Gamma_*$ .

[Figure 3c](#) shows that the contribution  $\Gamma_{*u}^{(0,1)}$  of the damped Kelvin wave represents a significant fraction of  $\Gamma_*$  (and  $\Gamma_{*u}$ ) except for small  $L_y$ . This relative contribution is larger than 60% for large  $L_x$ , which is consistent with the results in [Ipponen and Donner \(2021, see their Fig. 4\)](#), and it can be as low as one-third for small  $L_x$  and large  $L_y$ , which shows the importance of the low-level westerly jet associated with the damped Rossby waves for small  $L_x$ , even away from the limit  $L_y \rightarrow 0$ .

### c. Equatorial westerly jet

The main feature of the zonal asymmetry of the Gill circulation is the low-level westerly jet located at and around the heating center, which does not exist in the  $f$ -plane case. This feature is of particular interest for the potential coupling of circulation with explicitly modeled diabatic processes. Since such a low-level jet can modulate the surface turbulent heat fluxes, it could influence tropical intraseasonal variability ([Sobel et al. 2008, 2010](#)) and contribute to horizontal moisture advection, which is thought to contribute to the eastward propagation of tropical intraseasonal disturbances ([Maloney et al. 2010; Leroux et al. 2016](#)). The two cyclonic gyres that extend west of the heating center on both sides of the equator interact constructively to create this jet. As can be seen in [Fig. 1](#), as the scale of the heating decreases, the gyres become smaller, faster, and closer to the equator, which accelerates the low-level westerly jet and decreases its latitudinal extent. For infinitely small heating, the jet is infinitely fast at the equator, as established in [section 2d](#).

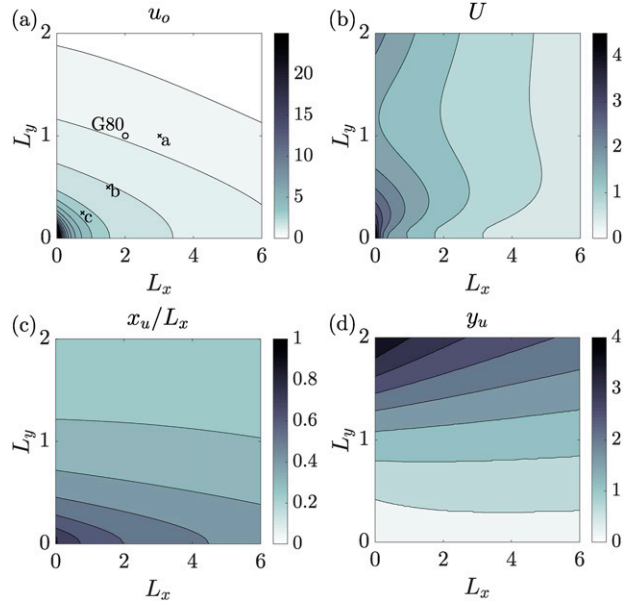


FIG. 5. Characteristics of the equatorial westerly jet in the Gill circulation: (a) westerly zonal velocity at the origin  $u_o$ ; the letters “a,” “b,” and “c” indicate the cases shown in [Figs. 1 and 2](#) and “G80” indicates the case discussed in [G80](#); (b) intensity  $U$  of the jet; (c) zonal extent  $x_u$  of the jet normalized by  $L_x$ ; (d) meridional extent  $y_u$  of the jet.

As metrics of this jet, we will study the low-level wind speed at the heating center:  $u_o = -u(0, 0)$  ( $u$  describes the first baroclinic mode, so that low-level winds have the opposite sign), the zonal extent of the jet  $x_u$  defined as the zonal coordinate at which  $u$  changes sign along the  $x$  axis:  $u(x_u, 0) = 0$ , the meridional extent of the jet  $y_u$  defined as the positive meridional coordinate at which  $u$  changes sign along the  $y$  axis:  $u(0, y_u) = 0$ , and the integrated intensity of the jet:  $U = - \int_{-y_u}^{y_u} u(0, y) dy$ , which describes the low-level eastward mass transport around the equator. [Figure 5](#) shows the sensitivity of these four metrics as a function of  $L_x$  and  $L_y$ .

The low-level equatorial wind  $u_o$  at the heating center decreases with both  $L_x$  and  $L_y$  (see [Fig. 5a](#)). It tends toward zero for large  $L_x$  or large  $L_y$ , and toward infinity if both  $L_x$  and  $L_y$  tend toward zero. We can also decompose  $u_o$  into a sum of contributions from the different modes:

$$u_o = \sum_{n=0}^{\infty} u_o^{(2n)} = \sum_{n=0}^{\infty} \left[ u_o^{(2n,1)} + u_o^{(2n,2)} \right], \quad (60)$$

with  $u_o^{(2n,1)}$  and  $u_o^{(2n,2)}$  the contributions of the first and second components of the response to the projection of the heating latitudinal distribution  $D$  on the  $n$ th symmetric latitudinal mode  $D_{2n}$ . [Appendix C](#) shows that there is a significant compensation between  $u_o^{(2n,2)}$  and  $u_o^{(2n,1)}$  for  $n > 0$  because the two gyres straddling the equator have opposite rotation (cyclonic vs anticyclonic) in the two components. We can write

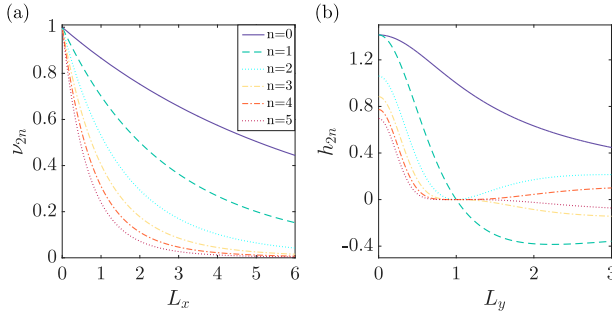


FIG. 6. Functions determining the sensitivity of the contributions  $u_o^{(2n)}$  to the westerly zonal velocity at the origin  $u_o$  for  $n \leq 5$ : (a)  $v_{2n}(L_x)$  gives the variation of  $u_o^{(2n)}$  with  $L_x$  and (b)  $h_{2n}$  gives the variation of  $u_o^{(2n)}$  with  $L_y$ .

$$u_o^{(2n)} = v_{2n}(L_x)h_{2n}(L_y), \quad (61)$$

with the variation in  $L_x$  (respectively,  $L_y$ ) encapsulated in the series of functions  $v_{2n}$  (respectively,  $h_{2n}$ ):

$$v_0(L_x) = -\frac{1}{2}q_0^{(0)}(0) + \frac{3}{2}q_2^{(0)}(0),$$

$$v_{2n}(L_x) = -\left(n - \frac{1}{4}\right)\frac{q_{2n}^{(2n)}(0)}{2n-1} + \left(n + \frac{3}{4}\right)q_{2n+2}^{(2n)}(0), \text{ for } n > 0, \quad (62)$$

$$h_0(L_y) = a_0(L_y)D_0(0) = \sqrt{\frac{2}{1+L_y^2}},$$

$$h_{2n}(L_y) = 2a_{2n}(L_y)D_{2n}(0) = \frac{(2n)!}{(2^n n!)^2} \left(\frac{1-L_y^2}{1+L_y^2}\right)^n \sqrt{\frac{8}{1+L_y^2}},$$

for  $n > 0$ . (63)

Figure 6 shows the functions  $v_{2n}$  and  $h_{2n}$  for  $n \leq 5$ . These show that the response to the forcing along  $D_0$  is the largest contribution to  $u_o$  except for  $L_x$  and  $L_y \rightarrow 0$ , but most latitudinal modes do contribute to the sensitivity of  $u_o$  to  $L_x$  and  $L_y$ . The functions  $v_{2n}$  include the two compensating effects of  $u_o^{(2n,1)}$  and  $u_o^{(2n,2)}$ . As a result of this compensation,  $v_{2n}(0) = 1$  is independent of  $n$ , and  $v_{2n}$  decreases toward 0 for  $L_x \rightarrow \infty$ . This decrease is faster for larger  $n$ , similarly to the functions  $\gamma_{2n}$  that describe the sensitivity of  $\Gamma_*$  to  $L_x$ .

The functions  $h_{2n}$  describe the sensitivity of  $u_o^{(2n)}$  to  $L_y$ , which is essentially dominated by the sensitivity of  $a_{2n}$  in terms of amplitude (see the similarity between Figs. 4b and 6b), but  $D_{2n}(0)$  contributes to the sign:  $D_{2n}(0)$ 's sign is given by  $(-1)^n$ , while  $a_{2n}$  is given by  $\left[\frac{1-L_y^2}{1+L_y^2}\right]^n$ ; as a result,  $h_{2n}$  is positive for all  $n$  if  $L_y < 1$  and for even  $n$  if  $L_y > 1$ ; it is negative for odd  $n$  if  $L_y > 1$ . As in the case of  $\Gamma_*$ , we find this distinction between two regimes on each side of  $L_y = 1$ :

- For  $L_y \leq 1$ , all latitudinal modes interact constructively to strengthen the low-level westerly jet. The amplitudes of functions  $h_{2n}$  decrease with  $L_y$ . For all  $n > 0$ ,  $h_{2n}$  and its  $(n-1)$  first derivatives are zero at  $L_y = 1$ ;  $h_{2n}$  also slowly decreases with increasing  $n$  for  $L_y = 0$  ( $h_{2n}(0) = [1 - (2n)^{-1}]h_{2n-2}(0)$ ).  $h_0$  is different, first because  $h_0(1) = 1$  (case with  $D = D_0$ ), and also because  $h_0(0)$  is not larger than  $h_2(0)$ : this results from the specificity of the first component of the response to heating along  $D_0$ , i.e., the damped Kelvin wave, which decreases the low-level westerly jet more efficiently than a competing gyre. The decrease of all  $h_{2n}$  with  $L_y$  in this regime results from the decrease in the amplitudes of projection coefficients  $a_{2n}$  with  $L_y$  (see Fig. 4b), which results directly from the smoother latitudinal distribution of heating with larger  $L_y$ . Moreover, the decrease in  $|a_{2n}|$  with  $L_y$  is larger for larger  $n$ , so that the relative contribution to  $u_o$  from latitudinal modes with large  $n$  decreases with  $L_y$ , which decreases its sensitivity to  $L_x$ .
- For  $L_y > 1$ , there is still a strong influence of the response of mode  $n = 0$ , and the influence of modes with larger  $n$  is complex. Because  $h_{2n}$  changes sign for each increment in  $n$ , there is considerable compensation between the contributions from successive latitudinal modes. For even  $n$ ,  $h_{2n} > 0$  and  $u_o^{(2n)}$  decreases with increasing  $L_x$ ; for odd  $n$ ,  $h_{2n} < 0$  and  $u_o^{(2n)}$  increases with increasing  $L_x$  ( $|u_o^{(2n)}|$  decreases), which reduces the sensitivity of  $u_o$  to  $L_x$ . The sensitivity of  $|h_{2n}|$  to  $L_y$  is still controlled by that of  $a_{2n}$ . The projection coefficient  $a_0$  decreases as  $(1+L_y^2)^{-1/2}$ , and, for  $n > 0$ ,  $a_{2n}$  increases from zero for  $L_y = 1$  to a maximum for a value of  $L_y$  that increases with  $n$ , because  $D$  projects more and more onto latitudinal modes that have significant amplitude farther and farther away from the equator as  $L_y$  increases. As a result, the contribution to  $u_o$  from latitudinal modes with  $n > 0$  comes largely from a subset of modes with similar  $n$ , with significant compensation between them, and as a result, its sensitivity to  $L_y$  results mostly from the contribution of the latitudinal mode  $n = 0$ . For  $L_y \rightarrow \infty$ , the contributions of latitudinal modes with larger and larger  $n$  get relatively larger, but all projections coefficients  $a_{2n}$  tend rapidly to zero, so that  $u_o$  also tends to zero.

Figure 5c shows the eastward longitudinal extent  $x_u$  of the low-level westerly jet normalized by  $L_x$ . For small  $L_x$  and  $L_y$ ,  $x_u \sim L_x$ , which means that the westerly jet extends over the whole heating region at the equator.  $x_u$  decreases with  $L_y$  and increases significantly less than  $L_x$  if  $L_x$  is increased. For very large  $L_x$  or  $L_y$ ,  $x_u$  tends toward zero (not shown), which means that the zonal flow becomes more symmetrical in longitude with respect to the heating center, with low-level westerlies to the west and easterlies to the east. Figure 5d shows, on the other hand, that the latitudinal extent  $y_u$  of the low-level westerly jet increases mostly with  $L_y$ . For  $L_x \rightarrow 0$ ,  $y_u$  scales like  $2L_y$  for  $L_y \rightarrow 0$  and this scaling is approximately valid for larger values of  $L_y$  as long as  $L_x \rightarrow 0$ : the region of westerlies scales in latitude with the heating region. For  $L_x > 0$ ,  $y_u$  is

small but nonzero for  $L_y = 0$  and the latitudinal widening of the region of westerlies with increasing  $L_y$  is less pronounced than for  $L_x \rightarrow 0$ . As a result, while  $y_u$  increases slightly with increasing  $L_x$  for  $L_y \rightarrow 0$ , it decreases with  $L_x$  for  $L_y > 0.7$ . The sensitivities of  $y_u$  and  $u_o$  help explain that of the intensity  $U$  of the low-level westerly jet shown in Fig. 5b: as the velocity  $u_o$  at the center of the jet decreases with  $L_y$ , its latitudinal extent  $y_u$  increases, and as a result,  $U$  is not very sensitive to  $L_y$ . On the other hand,  $U$  decreases with  $L_x$  because of the dominant influence of  $u_o$ . Using Eq. (42) in section 2d, we can confirm the following scalings in the limit  $L_x, L_y \rightarrow 0$ :

$$u_o \sim \frac{2}{L_y}, \quad (64)$$

$$x_u \sim L_x, \quad (65)$$

$$y_u \sim 2L_y, \quad (66)$$

and

$$U \sim 2\sqrt{\pi}\text{erf}(1) + 4e^{-1}. \quad (67)$$

Note that the maximum westerly wind is located at the equator, west of the heating center (not shown). It is furthest from the heating center, at  $(-L_x, 0)$  for  $L_x \rightarrow 0$  (see section 2d).

#### 4. Summary and conclusions

In this article, we explore the scale sensitivity of the equatorial Gill circulation, focusing on characteristics of this circulation likely to couple it with the energy cycle: we study the sensitivity of the overturning circulation intensity (total upward/downward mass flux), which interacts with cloud processes, and the characteristics of the low-level westerly flow, which influences turbulent surface heat fluxes. In all our cases, we impose the same horizontally integrated diabatic heating in order to understand how the dynamical response of the atmosphere depends on how spatially concentrated this diabatic heating is. In this Part I, we study the case of diabatic heating symmetric about the equator (Part II studies asymmetric cases).

We find that the intensity of the overturning circulation decreases with both the longitudinal and the latitudinal extents of the diabatic heating. Part of this sensitivity can be explained by the diffusive effect of vertical energy transport on temperature perturbation; as a result, this perturbation  $T$  is spatially smoother than the diabatic heating  $Q$ . This diffusive effect is less efficient for large horizontal scales of the heating than small scales, because the anomalies of  $T$  directly forced by  $Q$  are smoother. This also means that the vertical motion is smaller for large scales than for small ones. This sensitivity is enhanced by the influence of rotation, which causes the rotational part of the horizontal winds to be larger, as evidenced by the off-equatorial gyres west of the heating region. Since the imposed diabatic heating powers both the divergent and rotational circulations, stronger rotational winds result in weaker divergent winds and less intense overturning circulation. These results suggest that the coupling of

the Gill circulation with the energy and hydrologic cycle would result in a stronger moisture-convergence feedback for small heating regions than for large ones.

As for the low-level westerly jet in the region of diabatic heating, we find that for most metrics, it is relatively smaller and weaker for large horizontal scales than for small ones. The velocity at the center of the jet decreases with increasing scales, the latitudinal and longitudinal extents of the jet increase with increasing scales, but less than the latitudinal and longitudinal scales of the diabatic heating. The total zonal mass flux in this jet decreases with the longitudinal scale of the diabatic heating and its sensitivity to the latitudinal scale is small. Overall these results suggest that, in the heating region, the coupling with surface turbulent heat fluxes would result in a decrease of surface fluxes in easterlies and an increase in westerlies via the wind-induced surface heat flux mechanism. Over most of the tropics where trade winds are dominant, this creates a negative feedback to a diabatic-heating perturbation. Over the equatorial Indian Ocean where winds are westerlies, this would create a positive feedback. The amplitude of this feedback would be larger for small heating regions than for large ones.

Whether the amplitude and pattern of these moisture-convergence and surface-flux feedbacks would allow to sustain or enhance a circulation is beyond the scope of this article since it would require explicit coupling with the hydrologic and energy cycles; our results provide insights into the scale sensitivity of such feedbacks.

Our results are significant in general for the steady or slowly evolving tropical circulations, for which the dynamical response is very similar to the steady response. In particular, they are relevant for the MJO, the fundamental mechanisms of which are still debated (Yano and Tribbia 2017; Rostami and Zeitlin 2019; Zhang et al. 2020; and references therein). While the dynamical signature of the MJO resembles the symmetric solution described in G80, its latitudinal scale is smaller, and the scale sensitivity of the overturning circulation combined with its coupling to the hydrologic cycle might contribute to explaining the MJO scale selection. Also, the MJO convective disturbances do grow in the equatorial westerlies of the Indian Ocean, and some studies have suggested that these background winds are crucial to their development (Sobel et al. 2008, 2010; Maloney et al. 2010; Leroux et al. 2016), particularly because of wind-induced surface-heat-flux feedback described above, but also because of horizontal moisture advection; the scale sensitivity of the low-level westerly jet suggests that such mechanisms are particularly active for perturbations of small horizontal extent, e.g., during the development of MJO disturbances.

The observed MJO and interannual climate variability provide multiple opportunities to evaluate whether the scale dependency of observed circulations responding to equatorial heating follows the sensitivity predicted by the Gill circulation. This will be the topic of further work.

**Acknowledgments.** The authors thank Jean-Philippe Duvel for his useful comments. The authors also acknowledge the support of the University of Auckland, and particularly financial support from its Faculty of Science in the



form a Ph.D. fellowship and a grant from the Faculty Research Development Fund. G.B. is also supported by the Glavish-Buckley Lectureship.

## APPENDIX A

### A Few Properties of the Parabolic Cylinder Functions $D_n$

The parabolic cylinder functions  $D_n$  are defined by the recursive Eq. (7). They also verify, as pointed out by G80 [their Eqs. (3.7) and (3.8)],

$$\frac{dD_n}{dy} + \frac{y}{2}D_n = nD_{n-1}, \quad (\text{A1})$$

$$\frac{dD_n}{dy} - \frac{y}{2}D_n = -D_{n+1}, \quad (\text{A2})$$

and they are solutions of the differential equations:

$$\frac{d^2D_n}{dy^2} + \left(n + \frac{1}{2} - \frac{y^2}{4}\right)D_n = 0. \quad (\text{A3})$$

$D_{2n}$  are even functions and  $D_{2n+1}$  are odd functions of  $y$ . We have

$$D_{2n+1}(0) = 0 = \frac{dD_{2n}}{dy}(0), \quad (\text{A4})$$

$$D_{2n}(0) = -(2n+1)D_{2n-2}(0) = \left(-\frac{1}{2}\right)^n \frac{(2n)!}{n!} = -\frac{dD_{2n+1}}{dy}(0). \quad (\text{A5})$$

Using Eqs. (A1) and (A2), we can also write

$$\int_{Y_1}^{Y_2} D_{n+1} dy = n \int_{Y_1}^{Y_2} D_{n-1} dy - 2[D_n(Y_2) - D_n(Y_1)]. \quad (\text{A6})$$

## APPENDIX B

### Contributions of the Latitudinal Modes to $\Gamma_*$

By using the expressions of  $w^{(2n,i)}$  ( $i = 1$  or  $2$ ) in Eq. (25) combined with the expressions of  $T^{(2n,i)}$  from Eqs. (23) and (24) we can write  $\Gamma_*^{(2n,i)}$  as

$$\Gamma_*^{(2n,1)} = a_{2n} \left( I_{2n} - \frac{\varepsilon}{2} \int_{-L_x}^{L_x} q_{2n}^{(2n)} dx [I_{2n} + 2nI_{2n-2}] \right), \quad (\text{B1})$$

$$\Gamma_*^{(2n,2)} = a_{2n} \left( I_{2n} - \frac{\varepsilon}{2} \int_{-L_x}^{L_x} q_{2n+2}^{(2n)} dx [I_{2n+2} + (2n+2)I_{2n}] \right), \quad (\text{B2})$$

for all  $n$ . We have used  $\int_{-L_x}^{L_x} F dx = 2$  and introduced the notation

$$I_{2n} = \int_{-4L_y}^{4L_y} D_{2n} dy \text{ for } n \geq 0 \text{ and } I_{-2} = 0.$$

The differential Eqs. (11) and (14) yield the following expressions for the integrals of the functions  $q_{2n}^{(2n)}$ :

$$\varepsilon \int_{-L_x}^{L_x} q_0^{(0)} dx = 2 - q_0^{(0)}(L_x), \quad (\text{B3})$$

$$\varepsilon \int_{-L_x}^{L_x} q_{2n}^{(2n)} dx = \frac{1}{4n-1} [4n-2 - q_{2n}^{(2n)}(-L_x)] \text{ for } n > 0, \quad (\text{B4})$$

$$\varepsilon \int_{-L_x}^{L_x} q_{2n+2}^{(2n)} dx = \frac{1}{4n+3} [2 - q_{2n+2}^{(2n)}(-L_x)] \text{ for all } n, \quad (\text{B5})$$

in which we have used  $q_0^{(0)}(-L_x) = 0$ ,  $q_{2n}^{(2n)}(L_x) = 0$  for  $n > 0$ , and  $q_{2n+2}^{(2n)}(L_x) = 0$  for all  $n$ .

Equation (A6) yields

$$I_{2n-2} = \frac{1}{2n-1} [I_{2n} + 4D_{2n-1}(4L_y)] \text{ and}$$

$$I_{2n+2} = (2n+1)I_{2n} - 4D_{2n+1}(4L_y). \quad (\text{B6})$$

Using Eqs. (B3)–(B6), Eqs. (B1) and (B2) can be rewritten:

$$\Gamma_*^{(0,1)} = \frac{q_0^{(0)}(L_x)}{2} a_0 I_0, \quad (\text{B7})$$

$$\Gamma_*^{(2n,1)} = \frac{q_{2n}^{(2n)}(-L_x)}{4n-2} a_{2n} I_{2n} - \frac{8n}{4n-1} a_{2n} D_{2n-1}(4L_y) \times \left[ 1 - \frac{q_{2n}^{(2n)}(-L_x)}{4n-2} \right] \text{ for } n > 0, \quad (\text{B8})$$

$$\Gamma_*^{(2n,2)} = \frac{q_{2n+2}^{(2n)}(-L_x)}{2} a_{2n} I_{2n} + \frac{4}{4n+3} a_{2n} D_{2n+1}(4L_y) \times \left[ 1 - \frac{q_{2n+2}^{(2n)}(-L_x)}{2} \right] \text{ for all } n. \quad (\text{B9})$$

By replacing  $q_{2n}^{(2n)}$  by its expression from Eqs. (17) and (19), and using  $q_{2n}^{(2n)} = (2n-1)q_{2n}^{(2n-2)}$ ,  $\Gamma_*^{(2n,i)}$  can be written as Eqs. (50) and (51).

The contribution  $\Gamma_{*u}^{(2n,i)}$  to  $\Gamma_*^{(2n,i)}$  from the zonal flow is simply the integral of the zonal velocity  $u^{(2n,i)}$  over the zonal boundary of the rectangle  $(2L_x, 8L_y)$  where it is not zero, multiplied by  $\pm a_{2n}$ . Using Eqs. (21), (23), and (24), it can be written as

$$\Gamma_{*u}^{(0,1)} = \frac{a_0}{2} q_0^{(0)}(L_x) I_0 = \Gamma_*^{(0,1)}, \quad (\text{B10})$$

$$\Gamma_{*u}^{(2n,1)} = -\frac{a_{2n}}{2} q_{2n}^{(2n)}(-L_x) [I_{2n} - 2nI_{2n-2}] \text{ for } n > 0, \quad (\text{B11})$$



$$\Gamma_{su}^{(2n,2)} = -\frac{a_{2n}}{2} q_{2n+2}^{(2n)} (-L_x) [I_{2n+2} - (2n+2)I_{2n}] \text{ for all } n. \quad (\text{B12})$$

The last two can be simplified using Eq. (B6) into

$$\Gamma_{su}^{(2n,1)} = \frac{q_{2n}^{(2n)} (-L_x)}{4n-2} a_{2n} [I_{2n} + 8nD_{2n-1}(4L_y)] \text{ for } n > 0, \quad (\text{B13})$$

$$\Gamma_{su}^{(2n,2)} = \frac{q_{2n+2}^{(2n)} (-L_x)}{2} a_{2n} [I_{2n} + 4D_{2n+1}(4L_y)] \text{ for all } n. \quad (\text{B14})$$

By replacing  $q_{2n}^{(2n)}$  by its expression from Eqs. (17) and (19), and using  $q_{2n}^{(2n)} = (2n-1)q_{2n}^{(2n-2)}$ ,  $\Gamma_{su}^{(2n,i)}$  can be written as in Eqs. (57) and (58).

## APPENDIX C

### Contributions of the Latitudinal Modes to $u_o$

By using the expressions of  $u^{(2n,i)}$  ( $i = 1$  or  $2$ ) in Eqs. (23) and (24) we can write  $u_o^{(2n,i)}$  as

$$u_o^{(0,1)} = -\frac{a_0}{2} q_0^{(0)}(0)D_0(0), \quad (\text{C1})$$

$$u_o^{(2n,1)} = -\frac{a_{2n}}{2} q_{2n}^{(2n)}(0)[D_{2n}(0) - 2nD_{2n-2}(0)] \text{ for } n > 0, \quad (\text{C2})$$

$$u_o^{(2n,2)} = -\frac{a_{2n}}{2} q_{2n+2}^{(2n)}(0)[D_{2n+2}(0) - (2n+2)D_{2n}(0)] \text{ for all } n. \quad (\text{C3})$$

Using Eq. (A5), we can express the linear combinations of latitudinal modes at  $y = 0$  as proportional to  $D_{2n}(0)$ :

$$u_o^{(2n,1)} = -\frac{a_{2n}}{2} q_{2n}^{(2n)}(0) \frac{4n-1}{2n-1} D_{2n}(0), \quad (\text{C4})$$

$$u_o^{(2n,2)} = \frac{a_{2n}}{2} q_{2n+2}^{(2n)}(0)(4n+3)D_{2n}(0), \quad (\text{C5})$$

for all  $n$ .  $u^{(0,1)}$  is the westward wind associated with the Kelvin wave response.  $u_o^{(2n,1)}$  is the westward equatorial branch of the anticyclonic gyres along the equator for  $n > 0$  and  $u_o^{(2n,2)}$  is the eastward equatorial branch of the cyclonic gyres along the equator. They both scale with  $n$  and there is considerable compensation between them; therefore it does not provide any insight to present them independently. Their sum yields Eq. (61).

## REFERENCES

- Abramowitz, M., and I. A. Stegun, 1964: *Handbook of Mathematical Functions with Formulas, Graphs, and Mathematical Tables*. 9th ed. Dover, 1046 pp.
- Adam, O., 2018: Zonally varying ITCZs in a Matsuno-Gill-type model with an idealized Bjerknes feedback. *J. Adv. Model. Earth Syst.*, **10**, 1304–1318, <https://doi.org/10.1029/2017MS001183>.
- Back, L. E., and C. S. Bretherton, 2009: On the relationship between SST gradients, boundary layer winds, and convergence over the tropical oceans. *J. Climate*, **22**, 4182–4196, <https://doi.org/10.1175/2009JCLI2392.1>.
- Battisti, D. S., E. S. Sarachik, and A. C. Hirst, 1999: A consistent model for the large-scale steady surface atmospheric circulation in the tropics. *J. Climate*, **12**, 2956–2964, [https://doi.org/10.1175/1520-0442\(1999\)012<2956:ACMFTL>2.0.CO;2](https://doi.org/10.1175/1520-0442(1999)012<2956:ACMFTL>2.0.CO;2).
- Bellon, G., and B. Reboredo, 2021: Scale sensitivity of the Gill circulation. Part II: Off-equatorial case. *J. Atmos. Sci.*, <https://doi.org/10.1175/JAS-D-21-0068.1>, **79**, 19–30.
- Bretherton, C. S., and A. H. Sobel, 2003: The Gill model and the weak temperature gradient approximation. *J. Atmos. Sci.*, **60**, 451–460, [https://doi.org/10.1175/1520-0469\(2003\)060<0451:TGMATW>2.0.CO;2](https://doi.org/10.1175/1520-0469(2003)060<0451:TGMATW>2.0.CO;2).
- Cauchy, A. L. B., 1821: *Cours d'analyse de l'École Royale Polytechnique: Analyse algébrique*. Vol. 1. Debure frères, 576 pp.
- Gill, A. E., 1980: Some simple solutions for heat-induced tropical circulation. *Quart. J. Roy. Meteor. Soc.*, **106**, 447–462, <https://doi.org/10.1002/qj.49710644905>.
- Hackley, W. A., and A. E. Gill, 1984: Some simple analytical solutions to the problem of forced equatorial long waves. *Quart. J. Roy. Meteor. Soc.*, **110**, 203–217, <https://doi.org/10.1002/qj.49711046314>.
- Hendon, H. H., and M. L. Salby, 1994: The life cycle of the Madden-Julian oscillation. *J. Atmos. Sci.*, **51**, 2225–2237, [https://doi.org/10.1175/1520-0469\(1994\)051<2225:TLCOTM>2.0.CO;2](https://doi.org/10.1175/1520-0469(1994)051<2225:TLCOTM>2.0.CO;2).
- Iipponen, J., and L. Donner, 2021: Simple analytic solutions for a convectively driven Walker circulation and their relevance to observations. *J. Atmos. Sci.*, **78**, 299–311, <https://doi.org/10.1175/JAS-D-20-0014.1>.
- Kiladis, G. N., K. H. Straub, and P. T. Haertel, 2005: Zonal and vertical structure of the Madden-Julian oscillation. *J. Atmos. Sci.*, **62**, 2790–2809, <https://doi.org/10.1175/JAS3520.1>.
- Krueger, A. F., and J. S. Winston, 1974: A comparison of the flow over the tropics during two contrasting circulation regimes. *J. Atmos. Sci.*, **31**, 358–370, [https://doi.org/10.1175/1520-0469\(1974\)031<0358:ACOTFO>2.0.CO;2](https://doi.org/10.1175/1520-0469(1974)031<0358:ACOTFO>2.0.CO;2).
- Leroux, S., and Coauthors, 2016: Inter-model comparison of sub-seasonal tropical variability in aquaplanet experiments: Effect of a warm pool. *J. Adv. Model. Earth Syst.*, **8**, 1526–1551, <https://doi.org/10.1002/2016MS000683>.
- Lin, J.-L., M. Zhang, and B. Mapes, 2005: Zonal momentum budget of the Madden-Julian oscillation: The source and strength of equivalent linear damping. *J. Atmos. Sci.*, **62**, 2172–2188, <https://doi.org/10.1175/JAS3471.1>.
- , B. E. Mapes, and W. Han, 2008: What are the sources of mechanical damping in Matsuno-Gill-type models? *J. Climate*, **21**, 165–179, <https://doi.org/10.1175/2007JCLI1546.1>.
- Lintner, B. R., G. Bellon, A. H. Sobel, D. Kim, and J. D. Neelin, 2012: Implementation of the Quasi-Equilibrium Tropical Circulation Model 2 (QTCM2): Global simulations and convection sensitivity to free tropospheric moisture. *J. Adv. Model. Earth Syst.*, **4**, M12002, <https://doi.org/10.1029/2012MS000174>.
- Madden, R. A., and P. R. Julian, 1971: Detection of a 40–50 day oscillation in the zonal wind in the tropical Pacific. *J. Atmos. Sci.*, **28**, 702–708, [https://doi.org/10.1175/1520-0469\(1971\)028<0702:DOADOI>2.0.CO;2](https://doi.org/10.1175/1520-0469(1971)028<0702:DOADOI>2.0.CO;2).
- Maloney, E. D., A. H. Sobel, and W. M. Hannah, 2010: Intraseasonal variability in an aquaplanet general circulation model. *J. Adv. Model. Earth Syst.*, **2** (2), <https://doi.org/10.3894/JAMES2010.2.5>.

- Matsuno, T., 1966: Quasi-geostrophic motions in the equatorial area. *J. Meteor. Soc. Japan*, **44**, 25–43, [https://doi.org/10.2151/jmsj1965.44.1\\_25](https://doi.org/10.2151/jmsj1965.44.1_25).
- Neelin, J. D., 1989: On the interpretation of the Gill model. *J. Atmos. Sci.*, **46**, 2466–2468, [https://doi.org/10.1175/1520-0469\(1989\)046<2466:OTIOTG>2.0.CO;2](https://doi.org/10.1175/1520-0469(1989)046<2466:OTIOTG>2.0.CO;2).
- , and N. Zeng, 2000: A quasi-equilibrium tropical circulation model—Formulation. *J. Atmos. Sci.*, **57**, 1741–1766, [https://doi.org/10.1175/1520-0469\(2000\)057<1741:AQETCM>2.0.CO;2](https://doi.org/10.1175/1520-0469(2000)057<1741:AQETCM>2.0.CO;2).
- Pazan, S. E., and G. Meyers, 1982: Interannual fluctuations of the tropical Pacific wind field and the Southern Oscillation. *Mon. Wea. Rev.*, **110**, 587–600, [https://doi.org/10.1175/1520-0493\(1982\)110<0587:IFOTTP>2.0.CO;2](https://doi.org/10.1175/1520-0493(1982)110<0587:IFOTTP>2.0.CO;2).
- Philander, S. G. H., 1983: El Niño Southern Oscillation phenomena. *Nature*, **302**, 295–301, <https://doi.org/10.1038/302295a0>.
- Pierrehumbert, R. T., and M. Hammond, 2019: Atmospheric circulation of tide-locked exoplanets. *Annu. Rev. Fluid Mech.*, **51**, 275–303, <https://doi.org/10.1146/annurev-fluid-010518-040516>.
- Rostami, M., and V. Zeitlin, 2019: Eastward-moving convection-enhanced modons in shallow water in the equatorial tangent plane. *Phys. Fluids*, **31**, 21701, <https://doi.org/10.1063/1.5080415>.
- Showman, A. P., and L. M. Polvani, 2010: The Matsuno-Gill model and equatorial superrotation. *Geophys. Res. Lett.*, **37**, L18811, <https://doi.org/10.1029/2010GL044343>.
- , and —, 2011: Equatorial superrotation on tidally locked exoplanets. *Astrophys. J.*, **738**, 71, <https://doi.org/10.1088/0004-637X/738/1/71>.
- Sobel, A. H., and C. S. Bretherton, 2000: Modeling tropical precipitation in a single column. *J. Climate*, **13**, 4378–4392, [https://doi.org/10.1175/1520-0442\(2000\)013<4378:MTPIAS>2.0.CO;2](https://doi.org/10.1175/1520-0442(2000)013<4378:MTPIAS>2.0.CO;2).
- , E. D. Maloney, G. Bellon, and D. M. Frierson, 2008: The role of surface heat fluxes in tropical intraseasonal oscillations. *Nat. Geosci.*, **1**, 653–657, <https://doi.org/10.1038/ngeo312>.
- , —, —, and —, 2010: Surface fluxes and tropical intraseasonal variability: A reassessment. *J. Adv. Model. Earth Syst.*, **2** (1), <https://doi.org/10.3894/JAMES.2010.2.2>.
- Stechmann, S. N., and H. R. Ogrosky, 2014: The Walker circulation, diabatic heating, and outgoing longwave radiation. *Geophys. Res. Lett.*, **41**, 9097–9105, <https://doi.org/10.1002/2014GL062257>.
- Yano, J.-I., and J. J. Tribbia, 2017: Tropical atmospheric Madden-Julian oscillation: A strongly nonlinear free solitary Rossby wave? *J. Atmos. Sci.*, **74**, 3473–3489, <https://doi.org/10.1175/JAS-D-16-0319.1>.
- Yu, J.-Y., C. Chou, and J. D. Neelin, 1998: Estimating the gross moist stability of the tropical atmosphere. *J. Atmos. Sci.*, **55**, 1354–1372, [https://doi.org/10.1175/1520-0469\(1998\)055<1354:ETGMSO>2.0.CO;2](https://doi.org/10.1175/1520-0469(1998)055<1354:ETGMSO>2.0.CO;2).
- Zeng, N., J. D. Neelin, and C. Chou, 2000: A quasi-equilibrium tropical circulation model—Implementation and simulation. *J. Atmos. Sci.*, **57**, 1767–1796, [https://doi.org/10.1175/1520-0469\(2000\)057<1767:AQETCM>2.0.CO;2](https://doi.org/10.1175/1520-0469(2000)057<1767:AQETCM>2.0.CO;2).
- Zhang, C., 2005: Madden-Julian oscillation. *Rev. Geophys.*, **43**, RG2003, <https://doi.org/10.1029/2004RG000158>.
- , Á. Adames, B. Khouider, B. Wang, and D. Yang, 2020: Four theories of the Madden-Julian oscillation. *Rev. Geophys.*, **58**, e2019RG000685, <https://doi.org/10.1029/2019RG000685>.
- Zhang, Z., and T. N. Krishnamurti, 1996: A generalization of Gill's heat-induced tropical circulation. *J. Atmos. Sci.*, **53**, 1045–1052, [https://doi.org/10.1175/1520-0469\(1996\)053<1045:AGOGHI>2.0.CO;2](https://doi.org/10.1175/1520-0469(1996)053<1045:AGOGHI>2.0.CO;2).